IEEE Robotics and Automation Letters (RA-L) paper, presented at ICRA 2023, London, UK. Cite as RA-L paper.

A Tensegrity-Based Inchworm-like Robot for Crawling in Pipes with Varying Diameters

Yixiang Liu, *Member, IEEE*, Xiaolin Dai, Zhe Wang, Qing Bi, Rui Song, *Member, IEEE*, Jie Zhao, *Member, IEEE*, and Yibin Li, *Member, IEEE*

***Abstract*—Most current in-pipe robots are usually designed for pipes of a specific size. In this paper, we propose a novel inchworm-like in-pipe robot based on the concept of tensegrity for moving in pipes with varying diameters. Firstly, a tensegrity-based robotic module capable of two kinds of shape change is designed. One kind is extension in the axial direction accompanied by contraction in the radial direction, which is the basis for the wave-like crawling movement of the in-pipe robot. The other kind is expansion in the radial direction while keeping changeless in the axial direction, enabling the module adaptable to pipes with different diameters. Then, the geometrical equilibrium configuration of the tensegrity module is determined, followed by kinematic analysis using force density method. By cascading three modules, the in-pipe crawling robot is developed. Finally, a series of experiments are performed to test the shape changeability and friction force of the tensegrity module, and the mobility, load capacity, and adaptability of the in-pipe robot. The results validate that the robot can crawl in horizontal pipes, vertical pipes, and elbow pipes under the control of a simple actuation sequence. Furthermore, the robot has the abilities to adapt to pipes with different diameters varying from 100 mm to 180 mm. It is suggested that the usage of tensegrity structures brings about higher adaptability, flexibility, and mobility to the in-pipe crawling robot.**

***Index Terms*—Biologically-Inspired robots, Soft Robot Materials and Design, Climbing Robots, Compliant Joints and Mechanisms**

Manuscript received: April 29, 2022; Revised July 11, 2022; Accepted August 17, 2022.

This paper was recommended for publication by Editor Yong-Lae Park upon evaluation of the Associate Editor and Reviewers' comments. This work was supported in part by the National Natural Science Foundation of China under Grant 52005293 and U20A20201, Shandong Provincial Natural Science Foundation under Grant ZR2020QE152, Key R&D Program of Hebei Province, China under Grant 20311803D, Key R&D Program of Shandong Province, China under Grant 2021CXGC011304, Research Project of the State Key Laboratory of Mechanical Transmissions, Chongqing University under Grant SKLMT-KFKT-202123, and Fundamental Research Funds of Shandong University under Grant 2021JCG001. (*Corresponding author: Qing Bi*)

Yixiang Liu, Xiaolin Dai, Zhe Wang, Rui Song, and Yibin Li are with the School of Control Science and Engineering, Shandong University, and Engineering Research Center of Intelligent Unmanned System of Ministry of Education, Jinan 250061, China (email: liuyixiang@sdu.edu.cn; {202134839, 202034894}@mail.sdu.edu.cn; {rsong, liyb}@sdu.edu.cn).

Qing Bi is with Volvo Construction Equipment Technology (China) Co., Ltd, Jinan 250001, China (e-mail: biqing_meng@126.com).

Jie Zhao is with the State Key Laboratory of Robotics and System, Harbin Institute of Technology, Harbin 150080, China (e-mail: jzhao@hit.edu.cn).

Digital Object Identifier (DOI): see top of this page.

I. Introduction

In every corner of our modern society, there are many kinds of pipelines that may encounter problems such as aging, corrosion and blockage. With increasing demands for automatic detection and maintenance of pipelines, in-pipe robot has become a research hotspot in the field of robotics [1]. The existing in-pipe robots can be roughly divided into spider robots [2], [3], snake robots [4-6], inchworm-like robots [7-9] and others according to the bionics they are based on. Among these categories, inchworm-like robots cause much attention from researchers because of their advantages including simple structure, easy control, flexible locomotion, and good adaptability [10].

Imitating the crawling behavior of inchworms, Qiao designed an in-pipe robot using self-locking mechanism, which improved the mobility of the robot in the pipe [11]. Luo proposed an earthworm-like crawling robot by employing rigid elements-based morphing structures that made the mechanism precisely controllable [10]. However, these traditional robots are made of rigid materials, which limits the compliance, flexibility and adaptability of the robots. In order to solve these problems, soft crawling robots are proposed increasingly. For instance, Boxerbaum used a braided mesh exterior to produce continuous wave peristaltic motion along the body of a worm-like robot [12]. Zou designed a pneumatically powered reconfigurable omnidirectional soft robot that is composed of nine modules arranged as a three by three matrix [13]. Zhang proposed an earthworm-like robot with enhanced locomotion capability by exploiting the extraordinary deformability of the Yoshimura-origami structure [14]. Lin developed a single-actuator in-pipe crawling soft robot consisted of a McKibben pneumatic actuator surrounded by three longitudinally arranged elastic ribbons [15]. Some inchworm-like soft robots that could move and turn in a complex tubular environment were also proposed in [16-18]. Generally speaking, soft in-pipe crawling robots still have some limitations. First, most soft in-pipe robots use artificial muscles for actuation. The external air supply makes it hard for the robots to be fully untethered. Second, the design and fabrication of soft in-pipe robots face many difficulties. And third, soft in-pipe robots usually have poor load capacity and require complex control strategies.

Tensegrity, as the conjunction of tension and integrity, is put forward by the American architect Fuller, inspired by the

heterogeneous mixture of compressive elements and tensile elements in the nature. Tensegrity structure is defined as a self-stressed skeletal structure that has continuous tensile members and discontinuous compressive members so that each member performs efficiently in producing a rigid form [19]. Combining the characteristics of both rigid structures and soft structures, tensegrity structures have many advantages, such as high strength-to-weight ratio, high compliance, adjustable stiffness, high adaptability, and high load capacity [20]. Therefore, this kind of structure has been widely used in architecture and structural engineering [21].

More importantly, the property of tensegrity structures has been demonstrated in biological tissues of different sizes, from the skeletal systems of humans and animals to the molecular structure of spider fiber, and to the cytoskeletons of red blood cells. For example, the bones and tendons of human shoulder joint and elbow joint are connected in a manner that the bones provide compressive load-carrying capacity and the tendons provide the required stabilizing tensions [22]. In recent years, tensegrity structures are attracting more and more attention in the field of robotics. Comprehensive state-of-the-art researches on tensegrity robotics have been reviewed in [23] and our previous article [24]. Owing to the inherent biological features, tensegrity structures are also used to design worm-like crawling robots. Rieffel simulated the crawling gait of a 15-bar tensegrity robot [25]. In [26], Orki built a model of caterpillar crawling using Assur tensegrity structures, and simulated 2D caterpillar locomotion. In [27], Friesen developed the modified prototype of a duct climbing tetrahedral tensegrity robot, DuCTTv2, based on the first prototype [28]. DuCTTv2 is the first fully functional duct climbing tensegrity robot, but still has a bulky structure with eight actuators and a total mass of 3.75 kg. Zappetti designed a crawling modular robot based on icosahedron tensegrity structures using manufacturing techniques [29]. Venkateswaran added tensegrity structures to a piping inspection robot and designed a virtual model for the robot similar to elephant trunk [30]. In [31], Böhm designed a worm-like mobile robot enabling in-pipe crawling locomotion based on a tensegrity structure. But its mobility is limited since the maximum inclination angle can be overcome for uphill crawling is only 20 degrees. Kobayashi developed a tethered tensegrity crawling robot for exploration driven by artificial muscles [32].

Inspired by the above literature, we propose a novel inchworm-like in-pipe robot based on the concept of tensegrity for moving in pipes with varying diameters. Our main contributions lie in that a tensegrity-based robotic module capable of two kinds of shape change is designed. One kind is extension in the axial direction accompanied by contraction in the radial direction, which is the basis for the wave-like crawling movement of the in-pipe robot. The other kind is expansion in the radial direction while keeping changeless in the axial direction, enabling the module adaptable to pipes with different diameters. By cascading three modules, the in-pipe crawling robot is developed and the prototype is manufactured. Experimental results demonstrate that the proposed in-pipe robot, with a compact structure, can crawl in horizontal, vertical, and elbow pipes under the control of a simple actuation sequence, and can also adapt to pipes with different diameters varying from 100 mm to 180 mm.

The rest of this paper is organized as follows. Section II introduces the working principle of the tensegrity-based inchworm-like in-pipe robot. Section III presents the design of in-pipe robot in detail. Section IV introduces the experiments on the robot prototype. And conclusion and future works are finally presented in Section V.

II. Mechanics of the Tensegrity-Based Inchworm-like In-pipe Robot

A. Principle of In-pipe Crawling Movement

The tensegrity-based inchworm-like in-pipe robot proposed in this paper mainly imitates the morphological and behavioral characteristics of earthworms. The structural system of earthworms could be interpreted as high-pressure hydraulic tube consisted of a stretchable membrane-like body wall, collagen fibers serving as cable reinforcement to the membrane, and compressed fluid [33]. The body wall composed of circular and longitudinal muscles influences body form by contraction, while the collagen fibers bear the bulk of mechanical forces. As shown in Fig. 1(a), under the actions of circular and longitudinal muscles, the earthworm moves forward through peristaltic motion, consisting of alternating extensions and contractions that is linked to thickening and thinning along the body [33]. The principle of the proposed inchworm-like robot crawling in pipe is shown in Fig. 1(b). The robot mainly includes three parts connected in series, i.e. head segment, mid segments, and tail segment. Each segment is able to change its shape by extending in the axial direction while contracting in the radial direction, or contracting in the axial direction while expanding in the radial direction. The head segment and tail segment act as a retainer by fixing the robot with the pipe wall closely, and the mid segments act as a propeller through axial extension. Through a complete motion cycle, the robot will move a step forward. The step length is dependent on the changeability of the axial length of each segment and the number of segments in the robot. For a robot with N ($N \geqslant 3$) segments, the step length is N-2 times of the change in the axial length of the mid segments. If the head of the robot is converted to the tail, and the tail is converted to the head, then reverse crawling of the robot can be realized. In addition, by adjusting the diameter of the segments, the robot is able to crawl in pipes with different diameters in the same means.

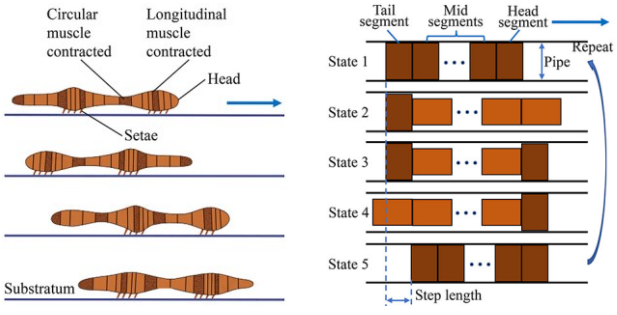

(a) (b)

Fig. 1. Peristaltic crawling pattern of (a) earthworms and (b) the robot.

B. Mechanics of the Tensegrity-Based Robotic Module

According to the requirements for shape changeability of the in-pipe crawling robot, a robotic module is proposed based on tensegrity structures. A typical tensegrity structure consists of rigid compressive struts suspended in a network of flexible strings in tension such the elements do not contact each other. Fig. 2 shows the structural model of the tensegrity-based robotic module. The tensegrity module is made up of 6 compressive elements and 15 tensile elements, connected at 12 nodes. The six compressive elements are divided into two groups. One group has only one central strut located at the axis of the module, and the other group has five surrounding struts with the same length located around the axis obliquely. There are no direct contact between any two compressive elements. The 15 tensile elements are also divided into two groups. One group has 10 identical radial springs that connect the central strut with the surrounding struts, and the other group has 5 identical axial springs that connect two adjacent surrounding struts. The connections between compressive elements and tensile elements are illustrated in the topological graphic of the tensegrity module in Fig. 3.

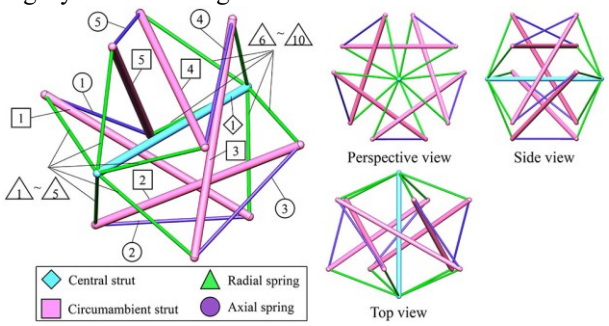

Fig. 2. Structural model of the tensegrity-based robotic module.

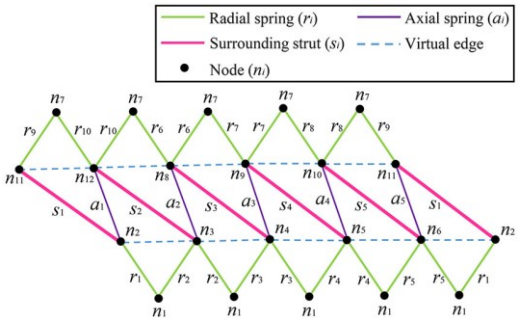

Fig. 3. Topological graphic of the tensegrity-based robotic module. The central strut connecting node n_1 and node n_7 is not shown.

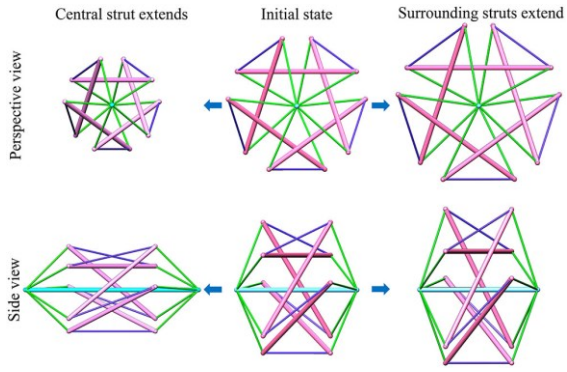

Fig. 4. Schematic diagram for shape change of the tensegrity module.

The whole tensegrity module is in an equilibrium configuration under the resultant forces of all compressive elements and tensile elements. When the length of any element is adjusted, the shape of the module will be induced to be changed. In this paper, the central strut and surrounding struts are designed as actuators with adjustable length. Thus, the robotic module is able to achieve two kinds of shape change. First, when the length of central strut increases, the surrounding struts will be pulled to move by the springs, then the module will extend in the axial direction while contract in the radial direction accordingly. Second, when the length of the five surrounding struts increase at the same time, the module will expand in the radial direction while keeping a fixed axial length. Fig. 4 presents the schematic diagram for shape change of the robotic module. It should be noted that the robotic module has an important feature that all the 10 ends of the 5 surrounding struts are always enveloped by a cylindrical surface. This allows the module to maintain good contact with the inner wall of a circular pipe, providing required friction forces for the robot during locomotion.

III. Design of the Tensegrity-Based Inchworm-Like In-Pipe Robot

A. Form-Finding of the Tensegrity-Based Robotic Module

The tensegrity-based robotic module is kept at static equilibrium under the complex internal forces generated by the tensile springs and compressive struts. This equilibrium may be affected by the material, stiffness, and length of any element. One of the most important and difficult issues in the design of the robotic module is the determination of its geometrical equilibrium configuration, known as form-finding. Therefore, a model of static equilibrium that yields equilibrium equations is required.

The static analysis of the tensegrity-based robotic module is based on the following assumptions: (1) Springs can only bear tension, while struts can only bear pressure; (2) Springs are linear elastic; (3) The frictions at the connection of elements are ignored; (4) The gravity of each element is ignored; (5) The internal forces on elements are in the axial direction.

The geometrical configuration of the tensegrity module can be uniquely determined by the connection relationship of all elements and nodes and the spatial coordinates of all nodes. The connection relationship represents the starting point and end point of each element, while the spatial coordinates involve its geometrical size. Suppose there are m elements (struts and springs) and n nodes in the tensegrity module. Then the connection relationship can be represented by the connectivity matrix $\mathbf{C}\in\mathbf{R}^{m*n}$. If element i connects nodes k and j, then the k-th and j-th columns for row i in the matrix $\mathbf{C}$ are set to 1 and -1 respectively, and all other entries are 0, i.e.:

$$\mathbf{C}(a,b)=\begin{cases}1 & \text{if } a=i, b=j\\ -1 & \text{if } a=i, b=k\\ 0 & \text{else}\end{cases} \tag{1}$$

The spatial coordinates of all nodes in the inertial coordinate system can be represented by the matrix $\mathbf{N}\in\mathbf{R}^{n*3}$. By

multiplying the matrixes **C** and **N**, the direction vector matrix of each element can be obtained as:

$$\mathbf{D} = \mathbf{CN} \tag{2}$$

The matrix **D** can be written in the form of column vectors as:

$$\mathbf{D} = \begin{bmatrix} \mathbf{u} & \mathbf{v} & \mathbf{w} \end{bmatrix} \tag{3}$$

where the column vectors **u**, **v**, **w** represent the projections of the element on *x*, *y* and *z* axes respectively.

The length of element *i* can be expressed as:

$$l_i^2 = u_i^2 + v_i^2 + w_i^2 \qquad i = 1, 2, ..., m \tag{4}$$

Based on force density method, the force density of element *i* that represents the unit force in unit length is:

$$q_i = k_i (l_i - l_{0,i}) / l_i \tag{5}$$

where k_i is stiffness, and $l_{0,i}$ is initial length of element *i*.

The force density of all elements forms a diagonal matrix:

$$\mathbf{Q} = \begin{bmatrix} q_1 & \dots & 0 & 0 \\ \dots & q_2 & \dots & 0 \\ 0 & \dots & \dots & \dots \\ 0 & 0 & \dots & q_m \end{bmatrix}_{m \times m} \tag{6}$$

By multiplying force density matrix and direction vector matrix, the force matrix of each element that represents the forces in *x*, *y* and *z* directions can be obtained as follows:

$$\mathbf{F} = \mathbf{QCN} \tag{7}$$

In the connectivity matrix, the elements corresponding to the nodes on the two ends of each element have non-zero values, and the remaining elements are zero. Therefore, the force of element *i* at node *j* is:

$$\mathbf{f}_i^j = \mathbf{C}_{:,j}^T \mathbf{F} \tag{8}$$

where $\mathbf{C}_{:,j}^T$ is the transpose of the elements in the *j*-th column of **C**.

Then the resultant forces on all nodes can be obtained as:

$$\mathbf{F} = \mathbf{C}^T \mathbf{F} = \mathbf{C}^T \mathbf{QCN} \tag{9}$$

By solving these nonlinear equations using the function of *fsolve* in MATLAB, the coordinates of all nodes that determine the geometrical configuration of the module can be obtained [34].

When designing the tensegrity module, the length of central strut and surrounding struts, the rest length and stiffness of axial springs and radial springs are given first of all. Then the geometrical equilibrium configuration of the module is solved from the above static equilibrium model, according to the flow diagram shown in Fig. 5(a). Fig. 5(b) shows the form-finding results of the tensegrity module in MATLAB. And the main parameters of the tensegrity module are given in Table I.

TABLE I
MAIN PARAMETERS OF THE TENSEGRITY MODULE

Parameter	VALUE
Length of central strut	140 mm
Length of surrounding strut	125 mm
Length of axial spring	100 mm
Length of radial spring	60 mm
Stiffness of axial spring	0.21 N/mm
Stiffness of radial spring	0.40 N/mm

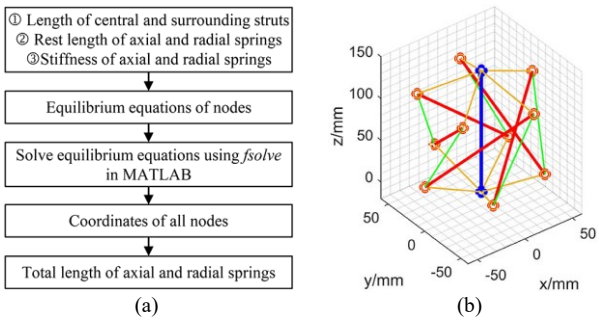

(a) (b)

Fig. 5. (a) Flow diagram for form-finding of the tensegrity module. (b) Geometrical equilibrium configuration of the tensegrity module.

B. Kinematic Analysis of the Tensegrity Module

Kinematic model describes the relationship between the shape change of the tensegrity module and its actuation. Assuming that the movement of the tensegrity module is a pseudo-static process, the kinematic analysis becomes to the form-finding of the module corresponding to different length of the central strut and surrounding struts. By changing the input values of the length of central strut or surrounding struts in Fig. 5(a) iteratively, the kinematics of the module can be obtained.

Firstly, the kinematics when the central strut actuates the tensegrity module are analyzed. In the current design, the maximum extension of the central strut is 75 mm. Fig. 6(a) shows the shape change of the tensegrity module during the extension of the central strut. It can be seen that when the central strut extends, contraction of the module in the radial direction is caused. Fig. 6(b) presents the changing curve of the module's diameter in relation to the extension of the central strut. It shows that the diameter of the module decreases from 108 mm to 72 mm as the central strut reaches maximum extension.

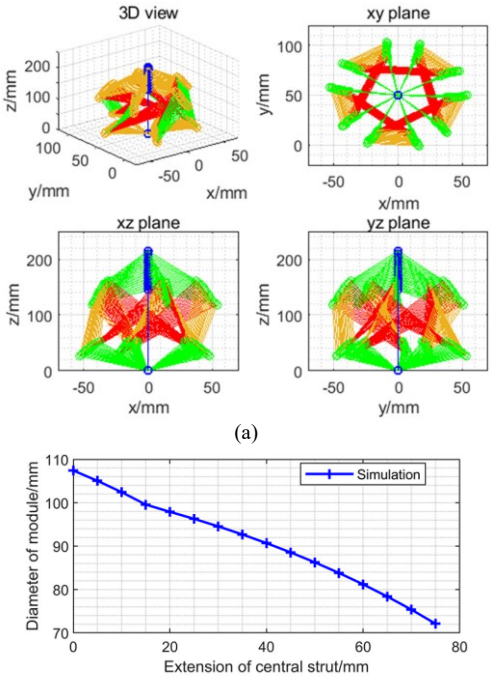

Fig. 6. Kinematics of the tensegrity module under the actuation of central strut. (a) 3D view and 2D views of the simulated tensegrity module during the extension of the central strut. (b) Changing curve of the diameter of the simulated tensegrity module in relation to the extension of the central strut.

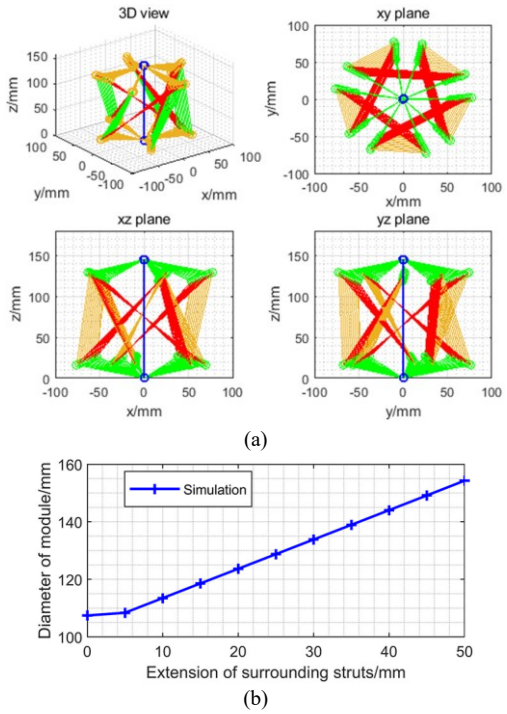

Fig. 7. Kinematics of the tensegrity module under the actuation of surrounding struts. (a) 3D view and 2D views of the simulated tensegrity module during the extension of the surrounding struts. (b) Changing curve of the diameter of the simulated tensegrity module in relation to the extension of surrounding struts.

Secondly, the kinematics when the surrounding struts actuate the tensegrity module are analyzed. The maximum extension of the surrounding struts is 50 mm. Fig. 7(a) shows the shape change of the tensegrity module during extension of the surrounding struts. It can be seen that when the surrounding struts extend at the same time, expansion of the module in the radial direction is caused. Fig. 7(b) presents the changing curve of the module's diameter in relation to the extension of surrounding struts. It shows that the diameter of the module increases from 108 mm to 155 mm as the surrounding struts reach maximum extension.

C. *Prototype of the In-pipe Crawling Robot*

A prototype of the tensegrity module is manufactured and assembled firstly based on the previous analysis. The central strut and surrounding struts are realized by commercially available motor-driven linear actuators. There are two main parameters to consider in product selection, that is, the stroke and the rated power. In this design, the central linear actuator has an initial length of 140 mm and a stroke of 75 mm, while the surrounding linear actuator has an initial length of 115 mm and a stroke of 50 mm. The two kinds of linear actuators have the same rated power of 3 W, providing a maximum pushing force of 64 N. The 10 radial springs are realized by standard tension springs with rest length of 45 mm, while the 5 axial springs are realized by standard tension springs with rest length of 70 mm. Fig. 8(a) shows the prototype of the tensegrity module. Its axial length (i.e., the distance between the two ends of the central linear actuator with the connectors included) is 180 mm, and its diameter (i.e., the diameter of the circle that envelopes all the ends of the five surrounding linear actuators) is about 141 mm. The main parameters of the prototype of the

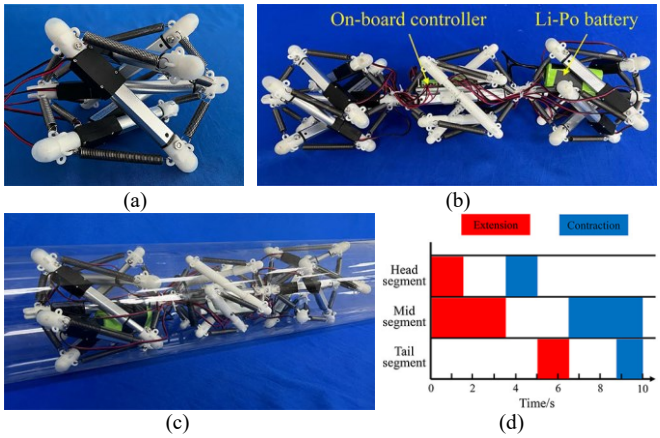

Fig. 8. (a) Prototype of the tensegrity-based robotic module. (b) Prototype of the untethered three-segmented in-pipe crawling robot. (c) The crawling robot in a transparent pipe made of polymethyl methacrylate. (d) Actuation strategy of the prototype based on a two-state-controller.

TABLE II
MAIN PARAMETERS OF THE PROTOTYPE OF THE TENSEGRITY MODULE

Parameter	VALUE
Minimum length of central linear actuator	140 mm
Maximum length of central linear actuator	215 mm
Minimum length of surrounding linear actuator	115 mm
Maximum length of surrounding linear actuator	165 mm
Rest length of axial spring	70 mm
Rest length of radial spring	45 mm
Stiffness of axial spring	0.26 N/mm
Stiffness of radial spring	0.42 N/mm

tensegrity module are given in Table II. It is obvious that there are some differences between the simulated model and the prototype. The differences mainly come from the simplification of the simulation, such as regarding each element as a line, and the connecting node as an ideal point, as well as the ignorance of gravity. For example, the diameter of the simulated tensegrity module in initial state is only 108 mm, which is 33 mm smaller than the prototype. But if we take the diameter of the linear actuators (i.e. 18 mm in this design) into account, the difference decreases to 15 mm.

On the basis of the tensegrity module, the in-pipe crawling robot is developed by connecting three modules together. It should be noted that only the head segment and tail segment use the above prototype. For the mid segment, it does not need to expand its diameter, so the five linear actuators are replaced by round rods made of nylon for structural simplification. Fig. 8(b) and (c) present the prototype of the in-pipe crawling robot. The robot is controlled by a custom designed on-board controller. The actuators and controller are powered by a 12 V Li-Po battery with a capacity of 3000 mAh. With the on-board controller and battery mounted on the robot, the robot is fully untethered, having a weight of about 1.3 kg. A personal computer is used as the top-level controller, which communicates with the on-board controller via Wi-Fi. Each module of the robot is controlled by a primitive two-state controller (i.e., extend and retract) shown in Fig. 8(d) in a repetitive pattern. The actuation strategy of each tensegrity module is programmed on the computer and then sent to the prototype.

IV. EXPERIMENTS

A. Shape Changeability Test

First of all, passive shape changeability is tested on the prototype of the tensegrity module by two experiments. In the first experiment, the tensegrity module is pressed by external loads. The results show that the module is deformed under the force, and restores its original shape without any damages caused once the force is removed. In the second experiment, the module is dropped from a height of 2 m. It shows that the module can absorb the impact from the ground using its intrinsic compliance without any caused damages. Fig. 9(a) shows the experimental results.

Then, active shape changeability is tested on the prototype of the tensegrity module by three experiments. In the first experiment, the central linear actuator extends until reaching maximum extension while the surrounding linear actuators keep fully contracted. The dimensions of the module are measured and recorded in the process. The results presented in Fig. 9(b) show that as the central linear actuator extends, the diameter of the module decreases consequently. The axial length of the module changes from 180 mm to 255 mm, and its diameter changes from 141 mm to 98 mm. As can be seen, the axial length increases by 41.6%, and the diameter decreases by 30.5%. In the second experiment, the five surrounding linear actuators extend until reaching maximum extension while the central linear actuator keeps fully contracted. The results show that the diameter of the module increases from 141 mm to 180 mm, about 21.7%, as presented in Fig. 9(c). In the third experiment, the surrounding linear actuators keep fully extended, and the central linear actuator extends out again to realize deformation of the module. As presented in Fig. 9(d), the diameter of the module decreases from 180 mm to 151 mm. Combining the above results, the total range of variation for the diameter of the robotic module is from 98 mm to 180 mm.

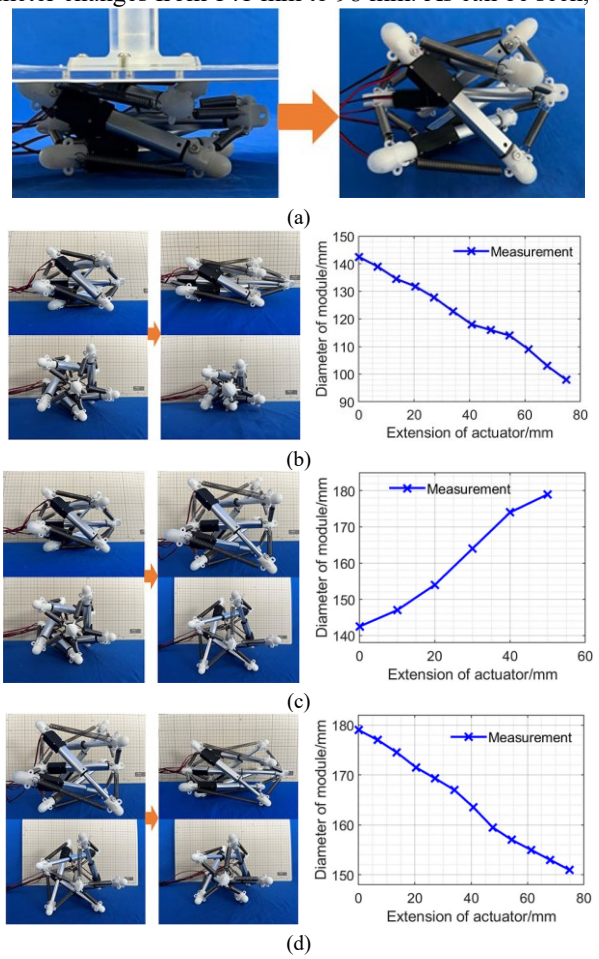

Fig. 9. Shape changeability test results of the tensegrity module. (a) The tensegrity module is pressed by external loads. The tensegrity module changes its shape as (b) the central linear actuator extends while the surrounding linear actuators keep fully contracted, (c) the surrounding linear actuators extend while the central linear actuator keeps fully contracted, and (d) the central linear actuator extends while the surrounding linear actuators keep fully extended.

B. Friction Force Test

This experiment aims to test the friction forces between the robotic module and the inner wall of the pipe. In the experiment, totally five kinds of pipes with different inner diameter values are adopted, specifically, 95 mm, 115 mm, 135 mm, 155 mm, and 175 mm. For each pipe, the diameter of the robotic module is adjusted to be 5 mm larger than the pipe by extending the central linear actuator or extending the surrounding linear actuators, such that the module can stay closely inside the pipe. Then a tension meter is used to pull one end of the module straight up along the axis of the pipe, and the pulling force during the process is recorded. The results presented in Fig. 10 indicate that the friction force becomes smaller as the diameter of the pipe increases. It also means the slippage is less likely to occur, and the load capacity may be higher when the robot moves in a smaller pipe. In the 95 mm pipe, the friction force is about 85 N; while in the 175 mm pipe, the friction force decreases to only 32 N, which suggesting that a minimum driving force of 32 N is required to enable the movements in a timely manner in the pipe.

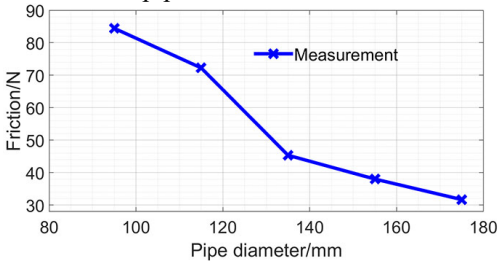

Fig. 10. Friction forces of the robotic module in pipes with different diameters.

C. Mobility Test

A series of experiments are performed to test the mobility of the in-pipe crawling robot, including moving in the horizontal pipe, in the vertical pipe, and in the elbow pipe. The adopted pipe has an inner diameter of 155 mm. In the first experiment, the robot moves in a horizontal pipe. The result shows that inchworm-like locomotion introduced in the previous section occurs in the pipe. As predicted, the expansion of the head and tail modules keeps the robot motionless in the pipe, and the extension of the mid module realizes a shift in the moving direction. The robot moves forward smoothly in the pipe without noticeable slippery. The step length is nearly the whole stroke of the central linear actuator, i.e. 75 mm.

In the second experiment, the robot moves in a vertical pipe.

The photograph sequence in Fig. 11(a) presents the result of the robot crawling in the vertical pipe from bottom to top. The result shows that the friction forces between the robot and the pipe are large enough to hold the robot, and the robot can dynamically lift up its own weight. Only slight slippery occurs during locomotion. The step length for upward crawling is about 65 mm.

In the third experiment, the robot moves in a 45 degrees elbow pipe. The result in Fig. 11(b) shows that the robot can follow the direction of the elbow pipe passively using its intrinsic compliance when moving forward, without being stuck at the turning. However, the step length decreases obviously owing to the increased friction forces at the turning. After tens of motion cycles, the robot manages to fully pass through the turning in the end. All these experiments verify the mobility of the in-pipe crawling robot.

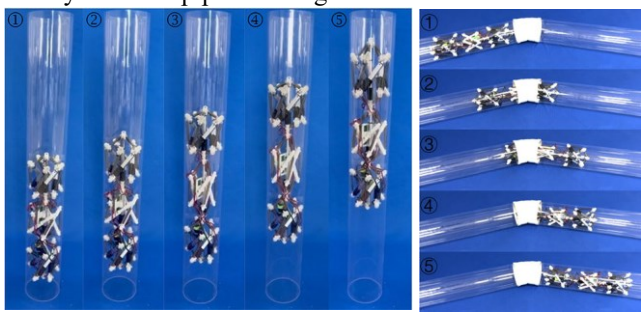

(a) (b)

Fig. 11. Mobility test results of the in-pipe crawling robot. (a) The robot crawls in a vertical pipe. (b) The robot crawls in a 45 degrees elbow pipe.

D. Adaptability Test

In this experiment, in order to evaluate the adaptability, the robot is tested to crawl in pipes with different diameters, including 95 mm, 115 mm, 135 mm, 155 mm, and 175 mm. Under each condition, the diameter of the robot is firstly adjusted to fit the corresponding pipe, and then the robot is controlled to move in the pipe horizontally and vertically respectively. Fig. 12 presents the measured step length in the experiment. The results show that the robot can adapt to different pipes successfully by adjusting the extension of surrounding linear actuators or central linear actuator, and can also realize continuous crawling under the same control sequence. Furthermore, the step length corresponding to crawling in each pipe varies. Specifically, when the robot moves in the 135 mm pipe, the step length is maximum, i.e. nearly the full stroke of the central linear actuator. When moving in the pipes with larger diameters such as 155 mm and 175 mm, the step length becomes a little smaller owing to the slight slippage caused by decreased friction forces. On the other hand, when the robot moves in the pipes with smaller diameters such as 95 mm and 115 mm, the step length decreases linearly. This is because the central linear actuator needs to extend some part out to shrink the radial size, and the stroke for crawling actuation is consequently decreased. In addition, the experimental results also indicate that when moving in the same pipe, the step length of vertical crawling is a little bit smaller than that of horizontal crawling because of the occasional slippage caused by the robot's weight.

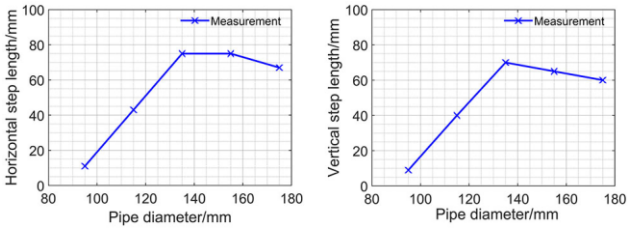

(a) (b)

Fig. 12. The step length when the robot crawls in pipes with different diameters.

E. Load Capacity Test

In order to evaluate the load capacity, the robot is tested to crawl in a horizontal pipe, pulling a certain load at the end of the robot that increases from 0 to 0.5 kg with an interval of 0.1 kg. The used pipes have a diameter of 115 mm, 135 mm, and 155 mm respectively. The step length is measured in each experiment. Fig. 13 presents the experimental results. It can be found that when crawling in 135 mm pipe, the step length decreases slightly because of the caused slippage as the external load increases. The step length is still as large as 60 mm under the load of 0.5 kg. When the robot crawls in a smaller pipe, i.e. the 115 mm pipe, since the friction forces between the robot and the pipe become larger, the effect of the external loads on the step length is not particularly obvious. Only very slight decrease occurs in the step length. When the robot crawls in a larger pipe, i.e. the 155 mm pipe, the friction forces between the robot and the pipe gets smaller. Therefore, the effects of the external loads on the robot's locomotion become more obvious, which means more serious slippage will be caused by heavier loads. As the external load increases to 0.5 kg, the step length of the robot crawling decreases from 75 mm to only 25 mm.

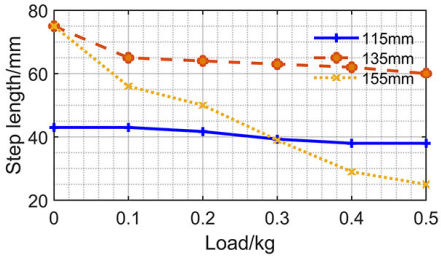

Fig. 13. The step length when the robot crawls with different loads.

V. Conclusion

This paper presents the proposal, design, analysis, and evaluation of an inchworm-like robot for crawling in pipes with varying diameters based on the concept of tensegrity structures. Effectiveness of the robot prototype is validated by a series of experiments. Compared with other in-pipe crawling robots, the proposed robot has several advantages. First, the robot has a very simple modular structure that results in easy fabrication, rapid assembly, and low cost of the robot. Second, the on-board controller and battery make the robot fully untethered, increasing the scope of workspace of the robot. Third, the robot has enhanced mobility. It has the abilities to support itself to crawl in vertical pipes, and can also pass through elbow pipes adaptively under the control of a simple actuation sequence. Fourth, the robot has better compliance and adaptability to the

changes in the sizes of pipes. The robot, with an initial diameter of 141 mm, is able to crawl in pipes with different diameters varying from 100 mm to 180 mm.

This research demonstrates the unique characteristics of tensegrity structures that may have great potential in the usage of new bio-inspired robots. However, there are still some limitations in the current research that affect the practical applications of the in-pipe crawling robot. Firstly, as an early version of prototype, there are no sensors and feedback signals on the robot for closed-loop control. Thus, the robot must be manually adjusted to fit the pipe with a fixed size. By equipping pressure/force sensors on the ends of surrounding linear actuators, it will be possible to realize automatic shape change based on the detected contact status between the robot and pipe wall. Secondly, waterproof and dustproof design of the robot body is not considered too much. More protection designs are required for the robot to handle harsh pipeline environment. Thirdly, active steering has not yet been achieved on the current robot. Higher maneuverability is of particular importance when faced with more complex pipelines such as T-junctions. In the future, essential improvements to the above problems must be made to move a step towards the practical applications of the robot.

REFERENCES

[1] Z. Zhang, X. Wang, S. Wang, D. Meng and B. Liang, "Design and Modeling of a Parallel-Pipe-Crawling Pneumatic Soft Robot," *IEEE Access*, vol. 7, pp. 134301-134317, 2019.

[2] J. H. Kim, H. J. Ko, S. H. Kim, M. G. Ji and J. B. Lee, "Intelligent system of the spider robot for the various moving functions," in *Proc. IEEE Int. Workshop Robot Human Interact. Commun*, 2009, pp. 226-231.

[3] A. Capua, A. Shapiro and S. Shoval, "SpiderBot: a cable-suspended walking robot," *Mech. Mach. Theory*, vol. 82, 2014, pp. 56-70.

[4] X. Qi, H. Shi, T. Pinto and X. Tan, "A Novel Pneumatic Soft Snake Robot Using Traveling-Wave Locomotion in Constrained Environments," *IEEE Robot. Autom. Lett.*, vol. 5, no. 2, pp. 1610-1617, April 2020.

[5] D. Shen, Q. Zhang, C. Wang, X. Wang and M. Tian, "Design and Analysis of a Snake-Inspired Crawling Robot Driven by Alterable Angle Scales," *IEEE Robot. Autom. Lett.*, vol. 6, no. 2, pp. 3744-3751, April 2021.

[6] B. Liao, H. Zang, M. Chen, et al. "Soft Rod-Climbing Robot Inspired by Winding Locomotion of Snake". *Soft Robot.*, vol. 7, no. 4, pp. 500-511, 2020.

[7] M. Liu, Z. Xu, J. J. Ong, J. Zhu and W. F. Lu, "An Earthworm-like Soft Robot with Integration of Single Pneumatic Actuator and Cellular Structures for Peristaltic Motion," in *Proc. IEEE/RSJ Intl. Conf. Intell. Robots and Syst.,* 2020, pp. 7840-7845.

[8] T. Kishi, M. Ikeuchi and T. Nakamura, "Development of a peristaltic crawling inspection robot for 1-inch gas pipes with continuous elbows," in *Proc. IEEE/RSJ Intl. Conf. Intell. Robots and Syst.*, 2013, pp. 3297-3302.

[9] T. Yamamoto, S. Sakama and A. Kamimura, "Pneumatic Duplex-Chambered Inchworm Mechanism for Narrow Pipes Driven by Only Two Air Supply Lines," *IEEE Robot. Autom. Lett.*, vol. 5, no. 4, pp. 5034-5042, Oct. 2020.

[10] Y. Luo, N. Zhao, Y. Shen and P. Li, "A Rigid Morphing Mechanism Enabled Earthworm-Like Crawling Robot," *ASME. J. Mech. Robot.*, vol. 15, no. 1, 011008, Feb. 2023.

[11] J. Qiao, J. Shang and A. Goldenberg, "Development of Inchworm In-Pipe Robot Based on Self-Locking Mechanism," *IEEE-ASME Trans. Mech.*, vol. 18, no. 2, pp. 799-806, April 2013.

[12] A. S. Boxerbaum, K. M. Shaw, H. J. Chiel and R. D. Quinn, "Continuous wave peristaltic motion in a robot," *Int. J. Robot. Res.*, vol. 31, no. 3, pp. 302-318, 2012.

[13] J. Zou, Y. Lin, C. Ji and H. Yang, "A reconfigurable omnidirectional soft robot based on caterpillar locomotion," *Soft Robot.*, vol. 5, no. 2, pp. 164-174, 2018.

[14] Q. Zhang, H. Fang and J. Xu, "Yoshimura-origami Based Earthworm-like Robot With 3-dimensional Locomotion Capability," *Front. Robot. AI*, vol. 8, Article 738214, 2021.

[15] Y. Lin, Y. X. Xu and J. Y. Juang, "Single-Actuator Soft Robot for In-Pipe Crawling," *Soft Robot.*, 2022, doi: 10.1089/soro.2021.0220.

[16] Y. Mano, R. Ishikawa, Y. Yamada and T. Nakamura, "Development of High-Speed Type Peristaltic Crawling Robot for Long-Distance and Complex-Line Sewer Pipe Inspection," in *Proc. IEEE/RSJ Intl. Conf. Intell. Robots and Syst.*, 2018, pp. 8177-8183.

[17] B. Zhang, Y. Fan, P. Yang, T. Cao and H. Liao. "Worm-Like Soft Robot for Complicated Tubular Environments," *Soft Robot.*, vol. 6, no. 3, pp. 399-413, June 2019.

[18] Z. Tang, J. Lu, Z. Wang, et al. "Design of a new air pressure perception multi-cavity pneumatic-driven earthworm-like soft robot," *Auton. Robot*, vol. 44, no. 2, pp. 267 – 279, 2020.

[19] C. Paul, F. J. Valero-Cuevas and H. Lipson, "Design and control of tensegrity robots for locomotion," *IEEE Trans. Robot.*, vol. 22, no. 5, pp. 944-957, Oct. 2006.

[20] A. Iscen, A. Agogino, V. SunSpiral and K. Tumer, "Flop and roll: Learning robust goal-directed locomotion for a Tensegrity Robot," in *Proc. IEEE/RSJ Intl. Conf. Intell. Robots and Syst.*, 2014, pp. 2236-2243.

[21] Y. Ushigome, R. Niiyama, K. Nishimura, T. Tanikawa and M. Hirose, "Archi/e Machina: Interactive architecture based on tensegrity," *Int. Conf. Virtual Syst. Multimedia*, 2010, pp. 55-62.

[22] R. E. Skelton and M. C. De Oliveira, Tensegrity systems. Springer, Boston, MA, 2009.

[23] D. S. Shah, J. W. Booth, R. L. Baines, K. Wang, M. Vespignani, K. Bekris and R. Kramer-Bottiglio, "Tensegrity Robotics" *Soft Robot.*, 2021, doi: 10.1089/soro.2020.0170.

[24] Y. Liu, Q. Bi, X. Yue, J. Wu, B. Yang and Y. Li, "A review on tensegrity structures-based robots," *Mech. Mach. Theory*, vol. 168, p.104571, 2022.

[25] J. A. Rieffel, F. J. Valero-Cuevas and H. Lipson, "Morphological communication: exploiting coupled dynamics in a complex mechanical structure to achieve locomotion," *J. R. Soc. Interface*, vol. 7, pp. 613-621, 2010.

[26] O. Orki, A. Ayali, O. Shai, and U. Ben-Hanan, "Modeling of caterpillar crawl using novel tensegrity structures," *Bioinspir. Biomim.*, vol. 7, p. 046006, 2012.

[27] J. M. Friesen et al., "The second generation prototype of a Duct Climbing Tensegrity robot, DuCTTv2," in *Proc. IEEE Int. Conf. Robot. Automat.*, 2016, pp. 2123-2128.

[28] J. Friesen, A. Pogue, T. Bewley, M. De Oliveira, R. Skelton, and V.Sunspiral, "DuCTT: A tensegrity robot for exploring duct systems," in *Proc. IEEE Int. Conf. Robot. Automat.*, Hong Kong, China, 2014, pp. 4222-4228.

[29] D. Zappetti, S. Mintchev, J. Shintake, D. Floreano, "Bio-inspired Tensegrity Soft Modular Robots," In: M. Mangan, M. Cutkosky, A. Mura, P. Verschure, T. Prescott, N. Lepora, (eds) Biomimetic and Biohybrid Systems. Living Machines 2017. *Lecture Notes in Computer Science*, vol. 10384. Springer, Cham.

[30] S. Venkateswaran, D. Chablat and P. Hamon, "An Optimal Design of a Flexible Piping Inspection Robot," *ASME J. Mech. Robot.*, vol. 13, no. 3, pp. 1-37, 2021.

[31] V. Böhm, P. Schorr, F. Schale, T. Kaufhold, L. Zentner and K. Zimmermann, "Worm-Like Mobile Robot Based on a Tensegrity Structure," in *Proc. IEEE Int. Conf. Soft Robot.*, 2021, pp. 358-363.

[32] R. Kobayashi, H. Nabae, G. Endo and K. Suzumori, "Soft Tensegrity Robot Driven by Thin Artificial Muscles for the Exploration of Unknown Spatial Configurations," *IEEE Robot. Autom. Lett.*, vol. 7, no. 2, pp. 5349-5356, April 2022.

[33] C. Hachem and A. Hanaor, "Folding Sleeves – Variations on a Theme of the Earthworm," *Int. J. Space Struct.*, vol. 20, no. 3, pp. 161-180, 2005.

[34] Y. Xie, "Analysis and Control about Rolling Motion of Spherical Tensegrity Robot," Thesis for the Degree of Master of Engineering in Mechanical Engineering, Harbin Institute of Technology, 2018.